Analysis of the electronic and local structure of amorphous SiN_x:H alloy films in terms of Si*K*, Si*L*, and N*K* x-ray emission bands

G. Wiech
Sektion Physik der Ludwig-Maximilians-Universität München, Geschwister-Scholl-Platz 1, 80539 München, Federal Republic of Germany

A. Šimůnek
Institute of Physics, Czech Academy of Sciences, Cukrovarnická 10, 16200 Prague, Czech Republic
(Received 31 August 1993)

We have studied silicon-nitrogen bonding states in amorphous SiN_x:H alloy films and in crystalline α-Si_3N_4 and β-Si_3N_4 by applying x-ray-emission spectroscopy (XES). We present x-ray Si *K*, Si *L*, and N *K* emission bands of alloy films covering the concentration range $0 \leq x \leq 2.03$ and identify spectral features on the base of *ab initio* calculations of all emission bands of β-Si_3N_4. The calculations delineate the role of Si 3*s*, 3*p*, and N 2*s*, 2*p* electrons in the bond and confirm the presence of silicon *d*-like electrons in the top region of the valence band. A comparison with available ultraviolet and x-ray photoelectron spectroscopy results is given. The position of the N 2*s* line observed in Si *K* and Si *L* emission bands of the alloys is analyzed in terms of the random-bond and random-mixture (RMM) models of nearest-neighbor structure of silicon atoms. The results unambiguously support the RMM structure of our samples and demonstrate that a detailed analysis of x-ray transitions observable in XES can yield unique and unconventional information about the local structure and the degree of phase separation in *a*-SiN_x:H alloy films.

I. INTRODUCTION

Silicon nitride films are widely used in a variety of electronic devices and the importance of amorphous hydrogenated SiN_x:H alloy films in the microelectronic and ceramic industries during the past ten years has prompted quite a number of studies conducted to determine structural and electronic properties of these alloys.[1–14] The composition x of the films affects the electronic structure and the device performance. Therefore their chemical bonding and electronic structure has been studied by applying ultraviolet and x-ray photoemission spectroscopy[1,9,11,14] (UPS and XPS), x-ray emission spectroscopy[3,5,8] (XES), infrared spectroscopy,[7] and extended x-ray-absorption fine structure (EXAFS).[4] Structural models and various calculational methods have been employed to determine the valence-band densities of states of amorphous silicon nitride (*a*-SiN_x) theoretically.[6,10,13] Quite recently, a review about a different parametrization of the valence and conduction bands of *a*-SiN_x was given by Robertson.[12]

The silicon-nitrogen bond combines covalent and ionic bonding, and according to the commonly accepted view of the nearest-neighbor structure, there are two different structural models. Both are based on silicon-centered tetrahedrons and in-plane triply coordinated nitrogen. The first model is the random-bonding model (RBM), in which a statistical distribution of five basic tetrahedral units Si-($Si_{4-n}N_n$) with $n = 0,1,2,3,4$ is assumed. The second model is the random-mixture model (RMM), in which the basic units Si-Si_4 and Si-N_4 predominate over the other units. Because Si-N_4 tetrahedrons and nitrogen triply coordinated with silicon atoms determine the short-range order of the crystalline forms of Si_3N_4 (α-Si_3N_4, β-Si_3N_4) the valence-band spectra of Si_3N_4 crystals have been studied, compared, and discussed with the spectra of *a*-SiN_x.[3,4,5,8,12]

The sensitivity of XES valence-band spectra to the local structure of solids and the direct information about electronic valence states with *p*-like and *s*- and *d*-like symmetry provided by Si *K* and Si *L* emission bands, respectively, have been found very useful for the analysis of the electronic structure of solids. In our previous work[5,8] we measured Si *K* and Si *L* emission bands of *a*-SiN_x:H for a few concentrations x. In this paper we present a complete set of x-ray emission bands (Si *K*, Si *L*, and N *K*) of a series of *a*-SiN_x:H alloy films (x=0, 0.35, 0.49, 0.67, 0.79, 0.92, 1.08, 1.33 and 2.03) and of crystalline α- and β-Si_3N_4. In addition, we present calculated Si *K*, Si *L*, and N *K* x-ray emission bands of β-Si_3N_4. We compared XES spectra with our calculations and with UPS valence-band spectra, and identified all features observable in XES and UPS valence-band spectra with respect to Si 3*s*, 3*p* and N 2*s*, 2*p* derived states. Moreover, we discussed structural models, RBM and RMM, in view of the x-ray valence-band spectra and the chemical shift of core levels.

The paper is organized as follows: In Sec. II we briefly describe the experiments, followed by a presentation and description of the spectra in Sec. III. In Sec. IV we discuss the electronic and real structure of our samples. A summary of the paper is given in Sec. V.

II. EXPERIMENT

A. Sample preparation

The samples of a-SiN_x:H with x varying in the concentration range $0 \le x \le 2.03$ were prepared from NH_3/SiH_4 gas mixtures by plasma deposition at low power (20 W) in a capacitive reactor system. Films of thicknesses $\sim 2\ \mu m$ were deposited onto copper substrates. The deposition parameters were $T_s = 250\,^{\circ}C$, $p = 0.1$ mbar, and flow 10 SCCM. Sample composition was determined by Auger electron spectroscopy and microprobe analysis. The content of hydrogen was obtained from effusion measurements and increased with increasing nitrogen content from 1.7 to 2.6×10^{22} atoms/cm^3 [corresponding to 10–20 at. % (Ref. 8)]. α- and β-Si_3N_4 were commercially available.

B. Measurement of XES spectra

For recording the Si K, Si L, and N K emission bands, three different spectrometers were employed. Details were reported in a recent paper,[15] therefore, only the most relevant facts will be mentioned here.

The Si K emission bands were measured with a high vacuum Johann-type spectrometer using fluorescence excitation. The radiation (characteristic radiation and bremsstrahlung of a tungsten anode; 10 kV, 200 mA) was dispersed by a quartz crystal ($10\bar{1}0$ plane) bent to a radius of 109 cm. The detector was a position-sensitive flow proportional counter with back gammon geometry operated at atmospheric pressure.[16] The energy resolution of the spectrometer was about 0.8 eV at 1835 eV.

The Si L emission bands were measured with a 2-m grazing incidence concave grating spectrometer using primary excitation (electron bombardment; 3 kV, 0.30–0.35 mA; c-Si_3N_4 up to 0.5 mA; focal spot ~ 10 mm^2). All spectra remained unchanged throughout the course of the measurement, i.e., the samples proved to be stable. The dispersing element was a blazed grating (3°31′, 600 lines/mm, angle of incidence 86°). The detector was a parallel-plate photoelectron multiplier.[17] The spectra were recorded in the step-scanning mode. The spectral resolution was about 0.3 eV.

The N K emission bands were measured with a 11.5-m grazing incidence concave grating spectrometer (holographic grating, 1200 lines/mm, angle of incidence 87.8°.[18] The spectrum of a rotating copper anode x-ray tube 9 kV, 1.2 A) was used for fluorescence excitation. The detector was a gas proportional counter (propane, 60 mbar) operated in the step-scanning mode. The energy resolution was about 0.6 eV at 390 eV.

III. RESULTS

A. Si K emission bands

Figure 1 shows the Si K emission bands of a-SiN_x:H for a series of concentrations in the range $0 \le x \le 2.03$ and of α- and β-Si_3N_4. The spectra consist of broadbands (maximum denoted B) without structural details and a line-shaped feature (denoted A), the so-called "N 2s-line." The bands develop gradually and exhibit small but distinct differences.

With increasing x the position of B is shifted to lower photon energy by about 2 eV, from 1836.4 eV ($x = 0$) to 1834.5 eV ($x = 1.33$). Practically no shift is observed in going from $x = 1.33$ to $x = 2.03$. The full width at half maximum (FWHM) is 4.3 eV for $x = 0$ and increases rapidly to ~ 5.15 eV for $x = 0.49$. Up to $x = 1.08$, it remains almost constant (5.1 ± 0.1 eV) and then again becomes smaller: 4.3 eV for $x = 1.33$ and 4.1 eV for $x = 2.03$. The position of the N 2s line A remains at the same energy 1823.15 ± 0.15 eV within the accuracy of the measurement; its intensity, however, increases with increasing x.

B. Si L emission bands

In Fig. 2 are shown the Si L emission bands of a-SiN_x:H for $0 \le x \le 2.03$ and of the crystalline α and β phases. With increasing x, the shape of the spectra develops gradually. The incorporation of nitrogen leads to a reduction of intensity in the region 91–93 eV, the broad maximum denoted B ($x = 0$, a-Si:H) becomes much narrower and develops into a line-shaped feature for $x = 1.33$. The shoulder of a-Si:H in the range 95–98 eV forms a peak (denoted D) for higher x. For $x > 1$, a new feature emerges at ~ 95 eV which forms a peak in the

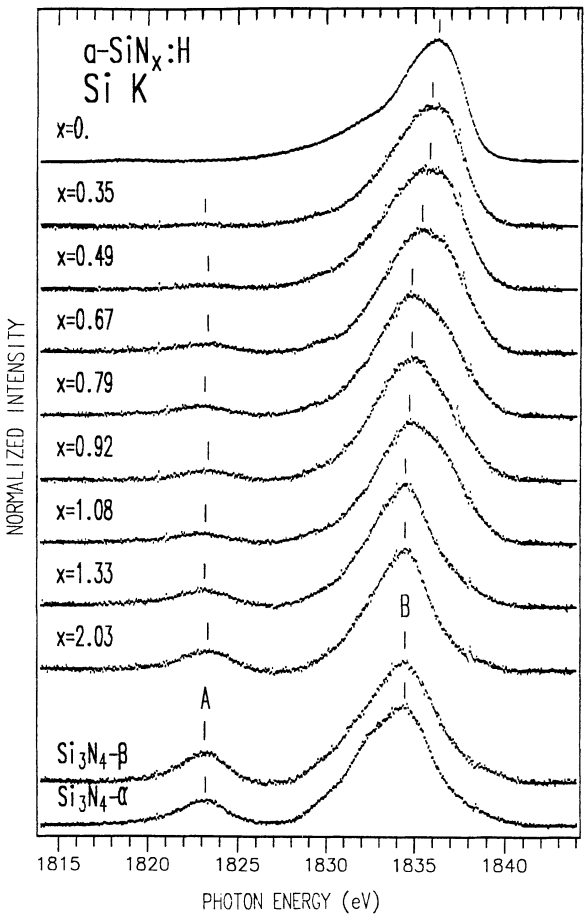

FIG. 1. Si K emission bands of a-SiN_x:H ($0 \le x \le 2.03$) and of α- and β-Si_3N_4.

emission bands of the crystalline phases (denoted *C*). The intensity of the line-shaped feature *A* (N 2*s* line) increases monotonously with increasing x up to $x=1.33$; for $x=2.03$, *A* has the same intensity. Within the accuracy of measurement, the positions of *A* (81.5±0.2 eV), *B* (89.8±0.1 eV), and *D* (96.7±0.1 eV) are constant. The position of *C* is at 94.6 eV.

The top of the emission band (as determined by linear extrapolation of the high photon energy edge) is approximately constant (~99.1–99.3 eV) for all x, while the bottom of the emission band (also determined by linear extrapolation) moves to higher photon energy from 84.7 eV ($x=0$) to 87.2 eV ($x=2.03$ and α- and β-Si_3N_4), i.e., the Si *L* emission bands become narrower by ~2.5 eV with increasing nitrogen content.

The Si *L* emission bands of nonstoichiometric silicon nitride samples SiN_x with different compositions x were studied by Nithianandam and Schnatterly.[3] Their analysis of spectra revealed that the samples were inhomogeneous, consisting of regions of *c*-Si and *a*-Si_3N_4. Therefore, the results of this study cannot be compared with our results in Fig. 2. Moreover, it may be mentioned that in our experimental setup the Si *L* emission bands of *a*-SiN_x:H are not affected by the fourth- and fifth-order N *K* emission bands.

C. N *K* emission bands

In Fig. 3 the N *K* emission bands are presented for $0.49\le x\le 2.03$, and for α-Si_3N_4. The spectra exhibit three distinct features *A*, *B*, and *D*, and a weak shoulder *C*. Within the accuracy of measurement, the position of the main peak *D* remains unchanged (392.9±0.1 eV) for all x, while *B* with increasing x is slightly shifted (~0.5 eV) to smaller photon energy. With increasing x (i) peak *D* becomes narrower, (ii) the intensity of the broad hump *B* becomes lower compared to *D*, and (iii) the high-energy falloff becomes steeper because the onset of energy is shifted towards smaller photon energy.

The differences between the N *K* bands for $x=1.33$ and 2.03 may be due to the replacement of Si-N bonds by N-H bonds. The presence of hydrogen in the *a*-SiN_x alloy films has been discussed in detail by Kärcher, Ley, and Johnson.[1] In our measurements we observe that hydrogen does affect only the N *K* emission bands, while the Si K and Si *L* emission bands are not affected. Therefore, we will not discuss the case of hydrogen in this paper.

D. Comparison of *a*-$SiN_{1.33}$:H with *c*-Si_3N_4

The Si *K*, Si *L*, and N *K* emission bands presented in Figs. 1, 2, and 3, respectively, also permit a comparison of the electronic structure of *a*-$SiN_{1.33}$ with that of *c*-Si_3N_4.

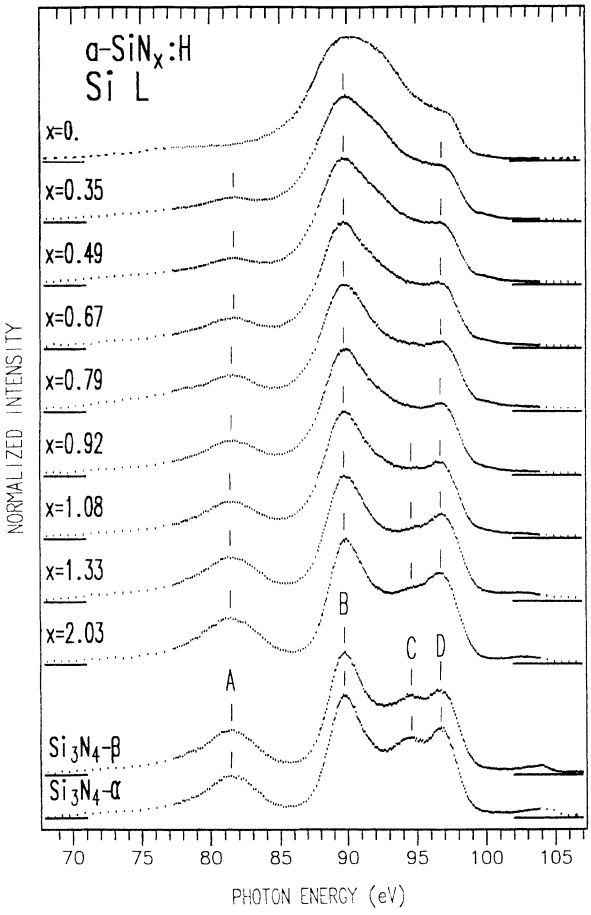

FIG. 2. Si *L* emission bands of *a*-SiN_x:H ($0\le x\le 2.03$) and of α- and β-Si_3N_4.

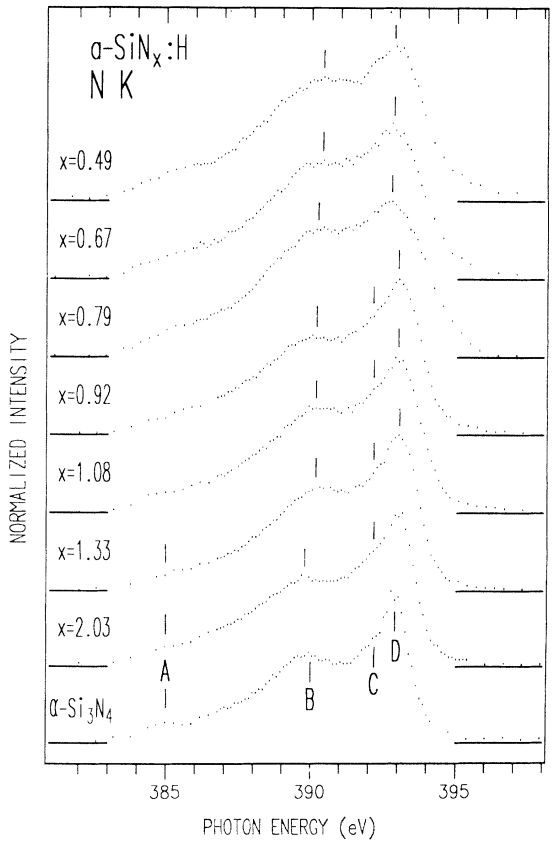

FIG. 3. N *K* emission bands of *a*-SiN_x:H ($0.49\le x\le 2.03$) and of α-Si_3N_4.

The Si K band of α-Si_3N_4 (Fig. 1) slightly differs from that of β-Si_3N_4 in that it has an additional weak shoulder at $\sim$1833 eV. The FWHM of the main bands is approximately the same ($\sim$4.9 eV), and the ratio of the intensities of the two main maxima, I_A:I_B, is very similar (0.22 and 0.23 for the α and β phases, respectively). On the whole, the Si K emission bands of β-Si_3N_4 and a-$SiN_{1.33}$:H are similar; the FWHM of a-$SiN_{1.33}$:H, however, is smaller ($\sim$4.4 eV) and the N 2s line is of lower intensity (intensity ratio $I_A:I_B \approx 0.14$). The results for $SiN_{2.03}$ are similar to those for $SiN_{1.33}$.

The Si L emission bands (Fig. 2) of α-Si_3N_4 and β-Si_3N_4 are very similar, features C and D being somewhat more pronounced in α-Si_3N_4 (α-Si_3N_4:$I_A/I_B/I_D = 34.9{:}100{:}72.2$; β-Si_3N_4:$I_A/I_B/I_D = 36.5{:}100{:}68.3$). For a-$SiN_{1.33}$:H ($I_A/I_B/I_D = 36.5{:}100{:}67.5$), features B and D are somewhat broader than in c-Si_3N_4 and feature C is very weak. The results for a-$SiN_{2.03}$:H again are very similar to those of a-$SiN_{1.33}$:H.

The Si L emission band of nearly stoichiometric silicon nitride (a-Si_3N_4) prepared by chemical vapor deposition (CVD) was also measured by Nithianandam and Schnatterly;[3] it shows the same features as the spectrum for $x = 1.33$ presented in Fig. 2. The Si L spectra of c-Si_3N_4 (Fig. 2) on the whole agree quite well with the Si L band of c-Si_3N_4 reported by Carson and Schnatterly[26] which, however, differs from our spectra on two points: (i) the N 2s line is considerably higher and (ii) the main peak is sharper in a-Si_3N_4 than in c-Si_3N_4.

On the whole, the N K emission bands of a-$SiN_{1.33}$:H and and α-Si_3N_4 are similar (Fig. 3); the intensity ratio I_D:I_B, however, is larger (1.67) for the crystalline sample than for the amorphous one (1.49), and in the amorphous sample features are broader and not as pronounced as in α-Si_3N_4.

Summarizing, we find that the Si K, Si L, and N K emission bands of a-$SiN_{1.33}$ and c-Si_3N_4 are quite similar. This indicates that (i) the electronic structure, and (ii) the local arrangement of Si and N atoms in a-$SiN_{1.33}$:H and c-Si_3N_4 must be very similar, and that (iii) the influence of hydrogen on the x-ray emission bands is marginal.

IV. CALCULATIONS OF X-RAY EMISSION BANDS OF β-Si_3N_4

The electronic-structure calculations of β-Si_3N_4 are based on the self-consistent pseudopotential method, and the plane-wave expansion of wave functions is used. The form of the potential and the electronic charge density is then fully determined by the structure and unbiased by any approximations affecting the symmetry of states. The local-density approximation is applied using the Hedin-Lundqvist interpolation formula[19] for the exchange and correlation potentials. The soft nonlocal pseudopotentials are generated employing the phase-shift technique.[20] The charge density and the crystal potential are iterated to self-consistency with an energy cutoff at 35 Ry; Brillouin-zone averages are sampled using three special $\vec{k}$ points[21] in the hexagonal Brillouin zone. The calculations are based on the experimental lattice constants with $a = 7.606$ Å and $c = 2.909$ Å. The resulting structure is in good accordance with the results of previous calculations.[12,22,23]

The Si K, Si L, and N K emission bands of β-Si_3N_4 are calculated in the dipole approximation. To obtain the matrix elements of the x-ray core-valence transitions in the pseudopotential approach, the dipole transition matrix element was split up into its radial and angular parts:

$$\langle \Psi_c(\vec{k},\vec{r}) | \vec{e}\cdot\vec{r} | \Psi_v(\vec{k},\vec{r}) \rangle = \langle \Psi_c | r | \Psi_v \rangle_{\text{rad}} \left\langle \Psi_c \left| \frac{\vec{e}\cdot\vec{r}}{r} \right| \Psi_v \right\rangle_{\text{ang}},$$

were $\vec{e}$ is the polarization vector. The core states N 1s, Si 1s, and Si 2p are localized in the core region of the atoms and therefore the $\Psi_c(\vec{k},\vec{r})$ functions are practically atomiclike. In the core region the valence electrons also have atomic character (the frozen-core approximation), and consequently the radial part of the matrix element $\langle \Psi_c | r | \Psi_v \rangle_{\text{rad}}$ is approximated by atomic calculations taking into account the new charge redistribution in the solid.[24] The angular part

$$\left\langle \Psi_c \left| \frac{\vec{e}\cdot\vec{r}}{r} \right| \Psi_v \right\rangle_{\text{ang}}$$

is adequately calculated by means of the pseudo-wavefunctions $\Psi_v(\vec{k},\vec{r})$.

The calculated spectra have been convoluted with a Lorentzian function whose width $w(E) = w_c + w \times (E/w_{\text{VB}})^2$ increases with energy E [measured from the top of the valence band (VB) with width w_{VB} (Ref. 25)]. For the parameter w, which takes into account the lifetime of holes in the VB, we used the value 1 eV; for w_c corresponding to the lifetime of the Si K, Si L, and N K core holes, we used the values 0.5, 0.3, and 0.3 eV, respectively. In addition, all curves were smeared by a Gaussian curve of FWHM 0.5 eV to take into account the spectral resolution of the spectrometers.

The calculated Si K, Si L, and N K emission bands of β-Si_3N_4 are presented on a common valence-band energy scale (the top of VB corresponds to 0 eV) in Fig. 4 together with the experimental results. In the case of the Si L emission band, contributions of the s- and d-like states are shown (Fig. 4, bottom). Since the three curves were convoluted separately, the sum "$s+d$" is not equal to the calculated Si L spectrum.

The alignment of experiment and theory in Fig. 4 was performed to achieve the best coincidence of spectral features; in addition the measured Si K and Si L bands were mutually alligned by the energy of the Si $K\alpha_1$ line of β-Si_3N_4 (1740.3 eV) applying the relation E (Si K) $= E$ (Si L) + E (Si $K\alpha_1$).

The calculated spectra are in very good agreement with our measurements and also with the Si L emission band reported by Carson and Schnatterly.[26]

V. DISCUSSION

A. Electronic structure

As shown in Figs. 1–3 and described in Sec. III D, the Si K, Si L, and N K emission bands for $x = 1.33$ are very

similar to the corresponding emission bands of β-Si_3N_4. This close relationship between the spectra of the amorphous and the crystalline phases also implies a close relationship between the corresponding valence electrons—Si 3*s*, Si 3*p*, N 2*s*, and N 2*p*—forming silicon-nitrogen bonds, and therefore justifies identifying the observed features in the spectra of the amorphous phase on the basis of the calculated emission bands of β-Si_3N_4.

β-Si_3N_4 contains two formula units in the unit cell, i.e., there are 32 occupied bands contributing to the emission bands. The lowest eight bands with binding energy ~ 17 eV (see Fig. 4) correspond to N 2*s* states. The electronic states in the energy interval 10 to 3.5 eV are formed by approximately 16 bands. In the 10–7-eV region, these states have mainly Si 3*s* character; with decreasing binding energy, the Si 3*s* character decreases in favor of the Si 3*p* and N 2*p* states. The valence states in the energy range 10–3.5 eV are Si-N bonding states, and only a small amount of Si 3*d*-like states forms a distinct feature in the Si *L* emission band at ~ 4 eV. This feature (denoted *C* in Fig. 2) is clearly observable at a photon energy of ~ 94.5 eV in both the α and β forms of crystalline Si_3N_4. The interpretation of its origin up to now was unclear.[26] The upper eight valence bands in the energy range 3.5–0 eV originate from a mixture of Si 3*s*, 3*p*, 3*d* and N 2*p* electrons localized on the nitrogen sites. Their nonbonding character is clearly visible in plots of the valence charge density published earlier by Liu and Cohen.[23] The localization of electrons on nitrogen atoms and the nonbonding N 2*p*-like character of states close to the top of the valence bands also explains the stable position of the main peak *D* of the N *K* emission bands of SiN_x:H in Fig. 3 for all concentrations *x*.

Actually, the Si *d*-like states do not play a significant role in the Si-N bond.[22,23] Due to the electronegativity of nitrogen, the majority of the valence charge is localized on the nitrogen atoms, and the charge transfer reduces the valence charge screening of silicon atoms. As a consequence of insufficient screening, the core levels of silicon are shifted to higher binding energy and the relative small valence charge on silicon exhibits not only *s*- and *p*- but also *d*-like character. The creation of *d*-like states on electropositive elements was also found in magnesium and aluminum oxides[27] and studied in detail for Si-O compounds.[15,24] Although the influence of these *d*-like electrons is marginal for the Si-N bond, *d*-like electrons are observable by local and orbital selective XES.[26,28]

To demonstrate the advantages of XES for identifying the origin of valence-band states in Fig. 5, we present x-ray emission bands of *a*-SiN_x:H ($x = 1.33$) together with available UPS ($x = 1.45$) spectra[1] of comparable concentration *x* on a common energy scale. For the alignment of UPS spectra with XES spectra, we used the binding energy of the core levels[1] and the well-defined character of N 2*s* and Si 3*s* peaks. In the concentration range $1.33 \leq x \leq 1.50$, the silicon atoms are bonded to four nitrogen atoms and therefore the core-level shift is the same for all silicon atoms, thus allowing us to compare UPS with XES spectra. The three features observable in UPS spectra and denoted *a*–*c* are clearly resolved by XES into Si 3*s*- (peak *a*), Si 3*p*- and N2 *p*- (*b*), Si 3*s*- and 3*d*- and N2*p*-(*c*) like states. The Si-N bond is formed mainly by electron states at energy positions *b* and *c*; the electron states at *c* are predominantly of nonbonding character.

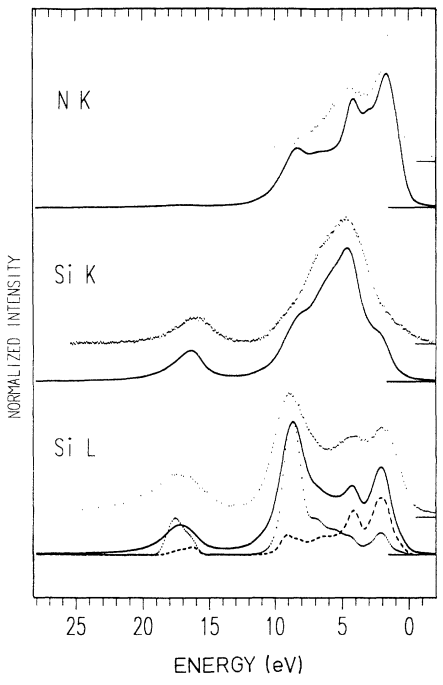

FIG. 4. Measured and calculated Si *K*, Si *L*, and N *K* emission bands of α-Si_3N_4. For the Si *L* emission band the contribution of *s*-like (· · · ·) and *d*-like (— — —) electrons is shown. The zero of the energy scale relates to the top of the valence band.

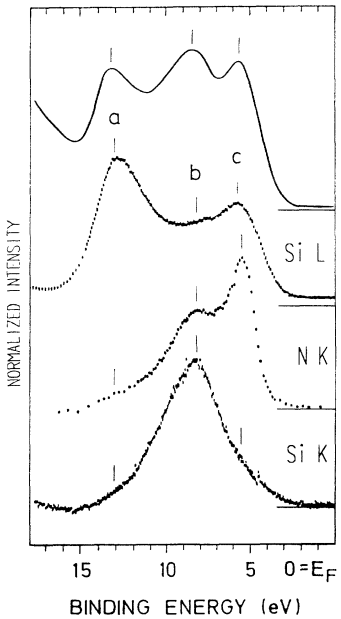

FIG. 5. X-ray emission bands (N *K*, Si *K*, and Si *L*) and photoelectron valence-band spectrum (Ref. 1) (UPS) for high concentrations *x* ($1.33 \leq x \leq 1.50$) aligned on a common energy scale.

character.

The evolution of the x-ray emission spectra of a-SiN_x:H alloys for eight different concentrations x is presented in Figs. 1–3; in each Figure the corresponding spectra of crystalline Si_3N_4 are also shown. The detailed description of the local orbital character of c-Si_3N_4 presented at the beginning of this chapter served as the basis for the identification of the spectral features of the a-SiN_x:H alloy films.

B. RBM and RMM structural models

In this chapter we use the x-ray spectroscopic results to study the local structure of our samples in view of RBM and RMM. Structural aspects were already treated in the photoemission spectroscopy (PES) studies of Kärcher, Ley, and Johnson,[1] further analyses of PES results were carried out by Guraya, Ascolani, and Zampieri[11] and Hasegawa, He, Inokuma, and Kurata.[14]

The ionicity of the Si-N bond and the charge transfer from the Si atoms to the more electronegative N atoms reduce the electronic screening on Si. As a result, the positive charge on the Si atoms creates a shift of all Si core levels towards higher binding energy. According to Kärcher, Ley, and Johnson,[1] the binding energy of the Si $2p$ level is 99.60 eV in a-Si and 102.80 eV in a-$SiN_{1.5}$. This 3.2-eV increase in binding energy goes monotonically with increasing x and is accompanied by a gradual increase of the width of the Si $2p$ line.

According to RBM, the bonding structure of a-SiN_x is composed of five basic bonding configurations Si-$(Si_{4-n}N_n)$ with $n=0,1,2,3,4$, and therefore five different bonding states of the Si atom are possible. By applying a curve-fitting procedure, the numerical analysis of the PES Si $2p$ line shape and binding energy yields a shift of the Si $2p$ level by 0.78 eV per Si-N bond.[1,11]

In RMM the alloy is considered to be composed of randomly dispersed clusters of a-Si and a-Si_3N_4 where each has a domain size of a few tetrahedral units Si-Si_4 ($n=0$) or Si-N_4 ($n=4$). It is supposed that in RMM other bonding units with $n=1$, 2, and 3 occur only at the boundary of clusters and therefore can be neglected. As a consequence, there are only two different Si $2p$ binding energies separated by 3.2 eV. Taking into account the energy of the Si $K\alpha_1$ lines (the $2p$-$1s$ transition) in silicon and Si_3N_4 crystals (1739.9 and 1740.3 eV, respectively; $\Delta E=0.4$ eV), we can estimate the shift of the Si $1s$ level to be about 3.6 eV (3.2+0.4 eV), i.e., about 0.90 eV per Si-N bond.

There is common agreement that nitrogen atoms in a-SiN_x are always fully coordinated by three Si atoms in a planar or near-planar configuration independent of concentration x. Infrared and Raman spectra suggest that the trivalent configuration of nitrogen is also retained in hydrogenated a-SiN_x:H alloys.[12] The absence of N-N bonds is understandable because of the very low stability of N-N single bonds compared to the bonds found in gaseous N_2 molecules.[12] As a consequence of the stable coordination of nitrogen, no chemical shift of the N $2s$ level is expected and found[1,9,10–13]:N $2s$-like states form a band (N $2s$ band) with a width of 4–5 eV at binding energy ~20 eV which does not change with the composition of samples.

The local character of x-ray dipole transitions implies that the N $2s$ lines in Figs. 1 and 2 correspond to transitions from the Si $3p$ and Si $3s$ and $3d$ contributions of the N $2s$ band to Si $1s$ and Si $2p$ core holes, respectively. In the Si K emission bands the center of gravity of the Si $3p$ contribution (peak A in Fig. 1) is at the photon energy 1823.2±0.2 eV; in the Si L emission band the center of gravity of the Si $3s$ and $3d$ contributions (peak A in Fig. 2) is at the photon energy 81.6±0.2 eV. This means (i) the energy position of A does not change with concentration for $x\geq 0.35$ and (ii) it has the same value for the amorphous and crystalline samples. Using the energy of the Si $K\alpha_1$ lines of c-Si (1739.9 eV) and c-Si_3N_4 (1740.3 eV), we find that the binding energy of the center of gravity of the Si $3s$ and $3d$ component of the N $2s$ band is higher than that of the Si $3p$ component by 1.3 eV [=1823.2−(1740.3+81.6)] in c-Si_3N_4 and therefore by 0.9 to 1.3 eV for all concentrations $x>0$. These values for the energy separation and the values for the widths of the N $2s$ lines in Figs. 1 (FWHM ~3.0 eV) and 2 (FWHM ~4.0 eV) yield a width of the N $2s$ band of 4–5 eV resulting from the Si $3p$ and Si $3s$ and $3d$ contributions [$\frac{1}{2}\times 3.0+(0.9$ to $1.3)+\frac{1}{2}\times 4.0$]. Therefore, the width of the N $2s$ band which is predominantly of N $2s$ character according to our x-ray measurements should have at least 4–5 eV.

Let us now discuss these experimental data in view of RBM and RMM local structures. Based on the PES and XES results, we present in Fig. 6 and energy-level diagram providing a summary of the valence-band and core-level energy positions in various structural configurations. Considering XES measurements, the diagrams for the RBM and RMM differ with respect to the position of the N $2s$ line (peak A) in the Si K as well as the Si L emission bands.

In the case of RBM there are five Si $1s$ and five Si $2p$ core levels separated by 0.90 and 0.78 eV, respectively. In XES emission bands of a-SiN_x:H alloys, four of these levels of the basic bonding units Si-$(Si_{4-n}N_n)$ with $n=1,2,3,4$ contribute to the N $2s$ line observable in the Si K and Si L emission bands for $x\geq 0.35$ (indicated by the arrows in Fig. 6). With increasing x, basic units with higher n should contribute more than the others,[1,11,14] and consequently the photon energy of the N $2s$ line should increase in both the Si K and Si L bands. This, however, is not observed, as Figs. 1 and 2 show. On the other hand, one could speculate that the photon energy of peaks A in Figs. 1 and 2 is independent of concentration x, if the centers of gravity of both the Si $3p$ and Si $3s$ and $3d$ contributions were shifted by the same amount as the corresponding core levels in Si-$(Si_{4-n}N_n)$ with $n=1,2,3,4$. According to this assumption and the fact that no chemical shift of the N $2s$ band is observed, the Si $3p$ and Si $3s$ and $3d$ contributions having a total width of 4–5 eV should move to higher binding energy *within* the N $2s$ band. This, however, would lead to a width of the N $2s$ band of at least 7 eV, contrary to all available data.

In the case of RMM the N $2s$ line arises only from the Si-N_4 basic unit and therefore feature A should stay at

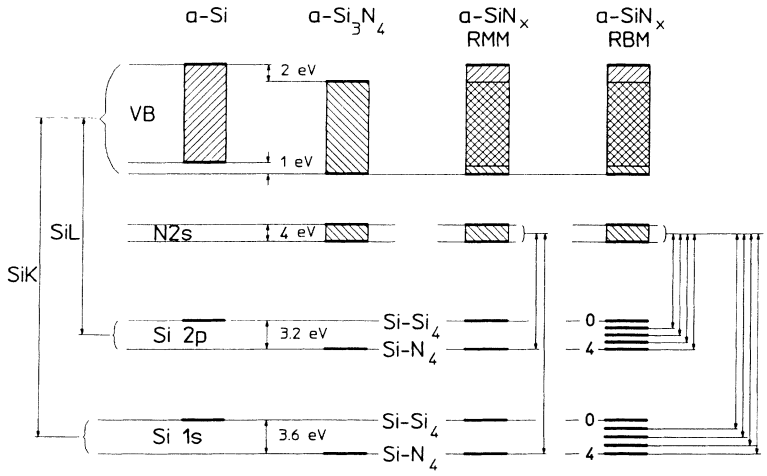

FIG. 6. Energy-level diagram of a-SiN_x:H compounds.

the same photon energy for all compositions of samples. Moreover, if the a-SiN_x samples are composed of Si as well as of Si_3N_4 clusters, the XES spectra should be similar to those resulting from a weighted superposition of spectra of a-Si and a-Si_3N_4.

The measured Si K and Si L emission bands of a-SiN_x:H presented in Figs. 1 and 2 display the characteristics mentioned above which are related to RMM structure of our samples: We do not observe any changes in photon energy of the N $2s$ lines (features A) in the Si K and Si L spectra. Moreover, the gradual development of shapes in Si K and Si L emission bands with increasing x also makes it evident that weighted superpositions of the spectra of a-Si and a-Si_3N_4 would be very similar to the corresponding measured spectra.

For the system a-SiO_x:H, $0 \leq x \leq 2.2$, we have calculated superpositions of measured emission bands of a-Si:H and a-SiO_2:H with weighting factors corresponding to x.[15] Contrary to the system a-SiN_x:H, we found that the structure of a-SiO_x:H can be considered as some mixture—depending on concentration x—of RBM and RMM structure.

Amorphous a-SiN_x:H films can be prepared over a wide range of concentrations x by various preparation techniques such as dc sputtering,[1] rf sputtering,[11] photochemical vapor deposition,[9] plasma-enhanced chemical vapor deposition,[29] glow discharge deposition,[4,7] and ion implantation.[30] For our samples prepared by plasma deposition at low power in a capacitive reactor system,[8] we have found that the RMM structure for samples with concentrations $x \geq 0.35$ is consistent with our experimental XES results. The RMM structure was also found in samples prepared by glow discharge deposition.[4,7] On the other hand, the results of XPS measurements of samples prepared by sputtering and chemical vapor deposition were analyzed on the basis of the RBM structure. Therefore it seems that (i) the microstructure of samples depends on the preparation techniques or (ii) the experimental techniques XPS and EELS which are more surface sensitive than XES, and EXAFS (Ref. 4) probe $Ls = v$ the more diverse bonds (RBM) on and close to the surface than the simpler composition (RMM) in the bulk.

VI. SUMMARY

In this paper we presented Si K, Si L, and N K emission bands of a-SiN_x:H alloy films measured in the concentration range $0 \leq x \leq 2.03$, and Si K and Si L emission bands of crystalline α-Si_3N_4 and β-Si_3N_4, and the N K emission band of α-Si_3N_4. We carried out *ab initio* calculations of the electronic structure and the Si K, Si L, and N K emission bands of β-Si_3N_4. The XES emission bands were compared with available UPS and XPS valence-band spectra. All features in the spectra were identified and attributed to Si $3s$, Si $3p$ and N $2s$, N $2p$ derived states. The calculations show that the silicon-nitrogen bond creates a small amount of Si d-like states in the upper part of the valence band which clearly show up in the Si L emission bands.

We analyzed the x-ray transitions in view of the RBM and RMM structure of a-SiN_x:H and found that our results for $x \geq 0.35$ support the RMM local structure of our samples. X-ray emission bands were used to distinguish between the local structure described by the random-bond and random-mixture models.

ACKNOWLEDGMENTS

We thank H.-O. Feldhütter, H. Langer, and U. Lepa for acquiring the experimental data, and Leibniz Rechenzentrum der Bayerischen Akademie der Wissenschaften, München, for generously putting computer time at our disposal. A. Šimůnek is greatly indebted to Deutsche Forschungsgemeinschaft for financial support.

[1] R. Kärcher, L. Ley, and R. L. Johnson, Phys. Rev. B **30**, 1896 (1984).

[2] E. Sacher and N. S. McIntyre, Phys. Rev. B **33**, 2845 (1986).

[3] V. J. Nithianandam and S. E. Schnatterly, Phys. Rev. B **36**, 1159 (1987).

[4] S. Mobilio and A. Filipponi, J. Non-Cryst. Solids **97&98**, 365 (1987).

[5] W. Zahorowski, R. Knop, H. Watanabe, and G. Wiech, J.

Non-Cryst. Solids **97&98**, 843 (1987).
[6]J. P. Xanthakis, S. Papadopoulos, and P. R. Mason, J. Phys. C **21**, L555 (1988).
[7]Z. Yin and F. W. Smith, J. Non-Cryst. Solids **114**, 489 (1989).
[8]G. Wiech, W. Zahorowski, A. Šimůnek, H. Mell, and G. Weiser, J. Non-Cryst. Solids **114**, 492 (1989).
[9]M. D. Khodja, A. LeCorre, C. Senemaud, A. Gheorghiu, M. L. Theye, B. Allain, and J. Perrin, J. Non-Cryst. Solids **114**, 498 (1989).
[10]S. S. Makler, G. Martins da Rocha, and E. V. Anda, Phys. Rev. B **41**, 5857 (1990).
[11]M. M. Guraya, H. Ascolani, and G. Zampieri, Phys. Rev. B **42**, 5677 (1990).
[12]J. Robertson, Philos. Mag. B **63**, 47 (1991).
[13]P. Ordejón and F. Ynduráin, J. Non-Cryst. Solids **137&138**, 891 (1991).
[14]S. Hasegawa, L. He, T. Inokuma, and Y. Kurata, Phys. Rev. B **46**, 12 748 (1992).
[15]G. Wiech, H.-O. Feldhütter, and A. Šimůnek, Phys. Rev. B **47**, 6981 (1993).
[16]W. Zahorowski, J. Mitternacht, and G. Wiech, Meas. Sci. Technol. **2**, 602 (1991).
[17]W. Schnell and G. Wiech, Microchim. Acta, Suppl. **7**, 323 (1977).
[18]E. Gilberg, M. J. Hanus, and B. Foltz, Rev. Sci. Instrum. **52**, 662 (1981).
[19]L. Hedin and B. I. Lundqvist, J. Phys. C **4**, 2064 (1971).
[20]J. Vackář and A. Šimůnek, Solid State Commun. **81**, 837 (1992).
[21]D. J. Chadi and M. L. Cohen, Phys. Rev. B **8**, 5747 (1973).
[22]S. Y. Ren and W. Y. Ching, Phys. Rev. B **23**, 5454 (1981).
[23]A. Y. Liu and M. L. Cohen, Phys. Rev. B **41**, 10 727 (1990).
[24]A. Šimůnek, J. Vackář, and G. Wiech, J. Phys. Condens. Matter **5**, 867 (1993).
[25]K. Schwarz and A. Neckel, Ber. Bunsenges. Phys. Chem. **79**, 1071 (1975).
[26]R. D. Carson and S. E. Schnatterly, Phys. Rev. B **33**, 2432 (1986).
[27]A. Šimůnek and G. Wiech, Z. Phys. B **93**, 51 (1993).
[28]E. P. Domashevskaya, Y. K. Timoshenko, V. A. Terekhov, E. N. Desyatirikova, E. Y. Bulycheva, and V. N. Seleznev, J. Non-Cryst. Solids **114**, 495 (1989).
[29]W. R. Knolle and J. W. Osenbach, J. Appl. Phys. **58**, 1248 (1985).
[30]S. Hasegawa and P. C. Zalm, J. Appl. Phys. **58**, 2539 (1985).